ORIGINAL ARTICLE

Accurate interpolation and contouring control algorithm based on FIR filters for the corner transition

Dongdong Li[1] · Liqiang Zhang[1] · Le Yang[1] · Jian Mao[1]

Abstract

In the process of high-speed machining, there are sharp corners at the joint of short lines. The vibration of cutting tools at the sharp corners will be severe, which will reduce the quality of machining surface and machining efficiency. For this problem, impulse response technology is proposed and applied. However, there is inevitable time delay in impulse response technology, which leads to the uncertainty of the maximum contour error of the corner. In order to further generate accurate reference motion trajectories, an accurate interpolation and contouring control algorithm based on FIR filters for the corner transition is proposed in this paper. According to the continuous short lines information in the CNC system, the rectangular velocity pulse signal of the short line is obtained. Initial rectangular velocity pulse is filtered to obtain third-order trajectory. In order to realize the continuous feed motion of short lines, the maximum feed velocity of short lines is constrained. Under the constraint of the maximum velocity limited, the maximum contour error of the corner is controlled by changing the overlapping time, and the accurate mathematical expression of the maximum contour error is reached. By using the FIR filters, the acceleration and jerk curves are generated from velocity pulse profiles. Through the experiment and simulation analysis, the algorithm proposed in this paper can determine the maximum contour error of the corner to realize smooth transition and reduce the machining path time by 7–10%. The proposed algorithm is proposed to achieve G^1 continuous acceleration and effectively improve the processing quality.

Keywords Contour error · FIR filters · Feed motion · Short lines

1 Introduction

In the process of manufacturing complex curves, curves are discretized into a series of continuous short lines. There will be high curvature or sharp corner at the junction of short lines. In order to generate a high-speed smooth path along the curve, corners must be planned.

The traditional interpolation algorithm can realize the continuous change of the speed between the short lines, the small amount of calculation is easy to apply. But the discontinuous acceleration at the corner will cause the vibration of the CNC machine tool and affect the quality of the processed parts. Some experts have given some solutions to solve this problem by using high-order spline curve, such as PH, NURBS, and Bezier [1–3].

The high-order spline can effectively reduce the vibration of the cutting tool and realize the uninterrupted feeding movement at the corner [4, 5], but the path speed planning of the spline needs to be done after the corner is transferred, and the calculation is complicated. Finite impulse response technology is proposed.

Finite impulse response technology has the characteristics of high efficiency and easy to be applied in hardware [6]. The technique generates a smooth feed profile through a filter. Starting with a simple reference signal, a series of integrators are combined with a suitable linear feedback controller to ensure that the feed motion is tracked in the fastest way. CS Chen et al. [7] proposed the finite impulse response filter can realize the real-time interpolation of feed and the generation of smooth trajectory. DI Kim et al. [8] proposed various digital filters were used to represent the convolution integral of the reference signal along the machining path to obtain the correct acceleration and deceleration algorithm, so that a single moving filter can obtain a constant acceleration, which can make the acceleration and speed transfer smooth. J W Jeon et al. [9] proposed that a single FIR filter was used to smooth the given feed signal by accurately calculating the coefficients of the filter. At the same time, this method was extended to all kinds of

✉ Liqiang Zhang
  zhangzlq@gmail.com

[1] School of Mechanical and Automotive Engineering, Shanghai University of Engineering Science, Shanghai 201620, People's Republic of China
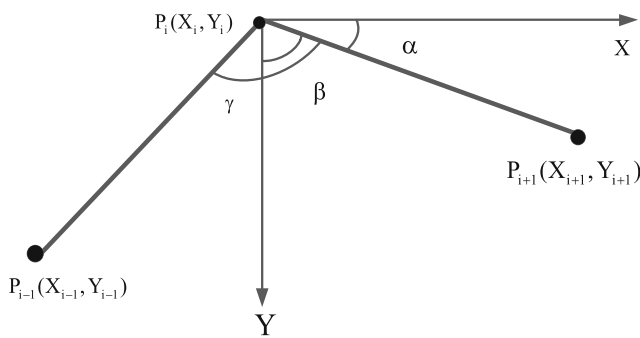
Fig. 1 Diagrammatic sketch of short lines

acceleration curves. B Sencer et al. [10] proposed that the cornering trajectory of the tool was generated by filtering the discontinuous axis speed command of FIR at the segment connection. P Besset et al. [11] proposed that the second-order trajectory was used to generate smooth jerk-constrained trajectories based on FIR filter. R Béarée et al. [12] proposed the FIR filter time method, and the jerk-limited profile was used to solve vibration problem by constant jerk-time. Y Altintas et al. [13] proposed that FIR filtering can produce unavoidable delay and induce large contouring errors in multi-axis motion; thus, contouring errors must be compensated.

In this paper, an accurate interpolation and contouring control algorithm based on FIR filters for the corner transition is proposed to determine the corner contour error and realize the smooth transition of the path of the corner. The maximum feed velocity constraint is established for a simple short reference path, and the third-order trajectory is generated by FIR filters. Then, the overlap time is determined by combining the speed at the corner and the given contour error. The maximum contour error of the corner is obtained in Sect. 2. The validity of proposed algorithms is tested by experiment in Sect. 3. The analysis is summarized in Sect. 4.

2 Maximum feed velocity constraint of continuous short lines

The schematic diagram of continuous short lines is shown in Fig. 1. The starting point of short line $P_{i-1}P_i$ coordinate is $P_{i-1} = [X_{i-1}, Y_{i-1}]$, and short-segment P_iP_{i+1} ends at $P_{i+1} = [X_{i+1}, Y_{i+1}]$. The junction point of linear segment $P_{i-1}P_i$ and P_iP_{i+1} is $P_i = [X_i, Y_i]$. V_{xm} is the maximum feed speed of X-axis. V_{ym} is the maximum feed speed of Y-axis. Maximum feed speed of short-segment $P_{i-1}P_i$ is V_{i-1m}. Maximum feed speed of short-segment P_iP_{i+1} is V_{im}. γ is the angle between short segments $P_{i-1}P_i$ and P_iP_{i+1}. α is the angle between short segments P_iP_{i+1} and X-axis. β is the angle between short segments P_iP_{i+1} and Y-axis. Parameters of short line segment can be computed as:

$$
\begin{aligned}
\overrightarrow{P_{i-1}P_i} &= (X_i - X_{i-1}, Y_i - Y_{i-1}) \\
\overrightarrow{P_iP_{i+1}} &= (X_{i+1} - X_i, Y_{i+1} - Y_i) \\
L_{i-1} &= \left| \overrightarrow{P_{i-1}P_i} \right| = \sqrt{(X_i - X_{i-1})^2 + (Y_i - Y_{i-1})^2} \\
L_i &= \left| \overrightarrow{P_iP_{i+1}} \right| = \sqrt{(X_{i+1} - X_i)^2 + (Y_{i+1} - Y_i)^2} \\
\gamma &= \arccos \left(\frac{\overrightarrow{P_{i-1}P_i} \cdot \overrightarrow{P_iP_{i+1}}}{\left| \overrightarrow{P_{i-1}P_i} \right| \times \left| \overrightarrow{P_iP_{i+1}} \right|} \right)
\end{aligned}
\tag{1}
$$

The direction of the feed speed of $P_{i-1}P_i$ and P_iP_{i+1} may be different, which may cause the change of the feed. For the relationship between short-segment P_iP_{i+1} and each axis, the following conditions can be defined as

$$
\begin{cases}
V_{im} \leq |V_{xm}/\cos(\alpha)| \\
V_{im} \leq |V_{ym}/\cos(\beta)|
\end{cases}
\tag{2}
$$

In order to achieve continuous feed motion, the short line needs to be completed within the sampling period of the driver. The maximum feed velocity needs to meet the following conditions:

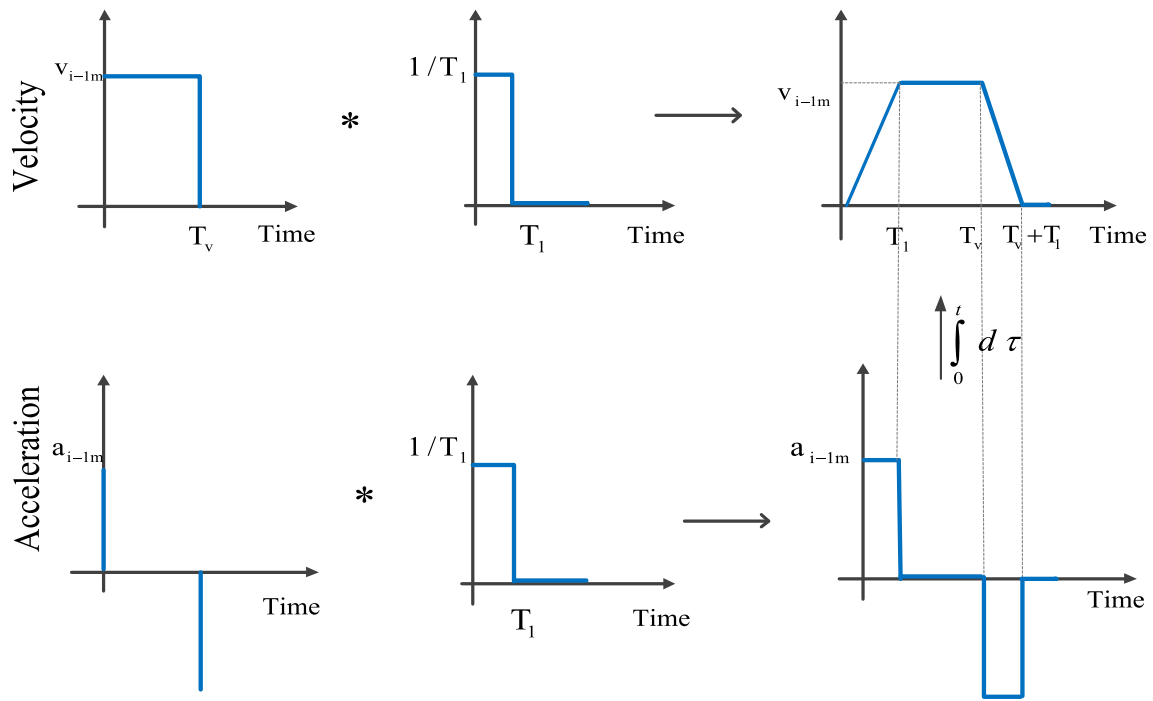**Fig. 2** A strategy for generating a third-order trajectory based on FIR
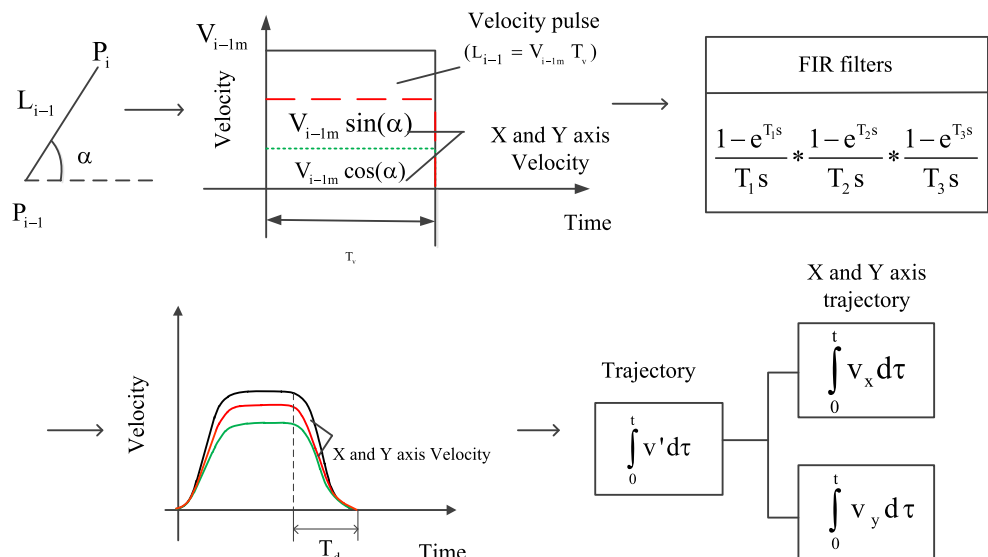
Fig. 3 Velocity and acceleration profiles of the first-order FIR filter
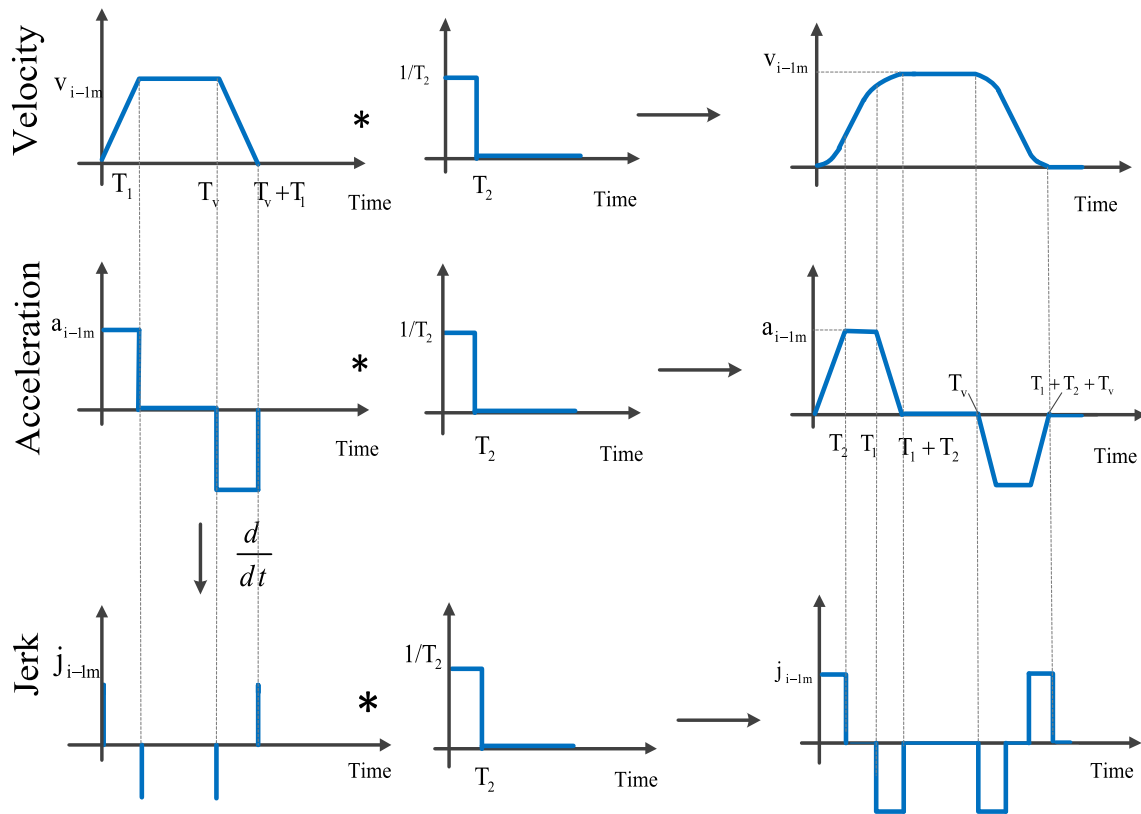
Fig. 4 Each parameter profiles of the second-order FIR filter

$$\begin{cases} V_{im}T \leq L_i \\ V_{im} \leq L_i/T \end{cases} \tag{3}$$

The maximum feed velocity of short line segment P_iP_{i+1} can be derived from Eqs. (2) and (3):

$$V_{im} = \min\{|V_{xm}/\cos(\alpha)|, |V_{ym}/\cos(\beta)|, L_i/T\} \tag{4}$$

2.1 Generation of high-order trajectory

Typically, "trapezoidal acceleration" or "trapezoidal jerk"–based feed profiling is used to generate smooth trajectories for high-speed and precision motion systems [11, 14]. This section mainly introduces the generation of third-order trajectory with FIR filters. As shown in Fig. 2, it is a strategy for generating a third-order trajectory based on FIR. L_{i-1} is the length of the short line segment, and T_v is duration time. The high-order trajectory is obtained by filtering the short-segment velocity rectangular pulse signal three times.

A first-order FIR filer is defined in Laplace by transfer function [8]:

$$M_i(s) = \frac{1}{T_i}\frac{1-e^{-sT_i}}{s} \tag{5}$$

where T_i is the time constant, representing the delay of ith FIR filters. Rectangular impulse response is evaluated by taking inverse Laplace transform of Eq. (5) as

$$m(t) = L^{-1}(M_i(s)) = \frac{u(t)-u(t-T_i)}{T_i} \quad \text{where } u = \begin{cases} 1 & t\geq 0 \\ 0 & t < 0 \end{cases} \tag{6}$$

The filter is realized by convoluting the input signal $v(t)$ with the defined FIR filters transfer function. Convolution is an integral operation, which can be used to describe the relationship between the input and output of linear time invariant system. The output signal can be obtained by convolution of the input signal and a function representing the characteristics of the system. The filtered velocity signal [15] can be expressed as

$$\begin{aligned} v'(t) &= v(t)*m(t) \\ &= \frac{1}{T_1}\int_0^t \Big([v(t)-v(\tau-T_v)] [u(t-\tau)-u(t-T_1-\tau)] \Big) d\tau \\ &= \frac{1}{T_1}\begin{bmatrix} \int_0^t v(t) u(t-\tau) d\tau - \int_0^t \Big([v(t) u(t-T_1-\tau) d\tau \\ -\int_0^t v(\tau-T_v) u(t-\tau) d\tau + \int_0^t v(\tau-T_v) u(t-T_1-\tau) d\tau \end{bmatrix} \end{aligned} \tag{7}$$

The duration time of a short line segment can be expressed as

$$T_v = L_{i-1}/V_{i-1m} \tag{8}$$

T_1 is the time constant of the 1st FIR filter, t is a time variable, T_{all} is the time required for overall motion duration. Under the condition of only considering $T_v > T_1$, the velocity expression of rectangular velocity curve after filtering once is written as

$$v'_{i-1m}(t) = \begin{cases} (V_{i-1m}/T_1)t & 0\leq t < T_1 \\ V_{i-1m} & T_1\leq t < T_v \\ V_{i-1m}/T_1(-t+T_v+T_1) & T_v\leq t < T_v+T_1 \\ 0 & T_v+T_1 < t \end{cases} \tag{9}$$

The acceleration profile in Fig. 3 can be written as

$$a'_{i-1m}(t) = \begin{cases} V_{i-1m}/T_1 & 0\leq t < T_1 \\ 0 & T_1\leq t < T_v \\ -V_{i-1m}/T_1 & T_v\leq t < T_v+T_1 \end{cases} \tag{10}$$

The process of filtering velocity and acceleration is shown in Fig. 3. The processing time of trapezoid velocity pulse signal and acceleration pulse signal is generated by convolution of rectangular pulse signal; the entire process is $T_{all} = T_v + T_1$, and delay time is $T_d = T_1$.

Under the condition of only considering $T_v > T_1 > T_2$, the velocity expression of the second filtering is written as

$$v_{i-1}''(t) = \begin{cases} \frac{1}{2}\frac{V_{i-1m}}{T_1T_2}t^2 & 0\leq t < T_2 \\ \frac{V_{i-1m}\,t}{T_1}-\frac{1}{2}\frac{V_{i-1m}T_2}{T_1} & T_2\leq t < T_1 \\ V_{i-1m}-\frac{V_{i-1m}}{2T_1T_2}(T_1+T_2-t)^2 & T_1\leq t < T_1+T_2 \\ V_{i-1m} & T_1+T_2\leq t < T_v \\ V_{i-1m}-\frac{1}{2}\frac{V_{i-1m}}{T_1T_2}(t-T_v)^2 & T_v\leq t < T_v+T_2 \\ \frac{1}{2}\frac{V_{i-1m}}{T_1T_2}\left(-2tT_2+T_2^2+2T_vT_2+2T_1T_2\right) & T_v+T_2\leq t < T_v+T_1 \\ \frac{1}{2}\frac{V_{i-1m}}{T_1T_2}(T_v+T_1+T_2-t)^2 & T_v+T_1\leq t < T_v+T_1+T_2 \\ 0 & T_v+T_1+T_2 < t \end{cases} \tag{11}$$

The acceleration profile in Fig. 4 can be written as

$$a_{i-1}''(t) = \begin{cases} \frac{V_{i-1m}}{T_1T_2}t & 0\leq t < T_2 \\ \frac{V_{i-1m}}{T_1} & T_2\leq t < T_1 \\ \frac{V_{i-1m}}{T_1}-\frac{V_{i-1m}}{T_1T_2}(t-T_1) & T_1\leq t < T_1+T_2 \\ 0 & T_1+T_2\leq t < T_v \\ -\frac{V_{i-1m}}{T_1T_2}(t-T_v) & T_v\leq t < T_v+T_2 \\ -\frac{V_{i-1m}}{T_1} & T_v+T_2\leq t < T_v+T_1 \\ -\frac{V_{i-1m}}{T_1}+\frac{V_{i-1m}}{T_1T_2}\left(t-(T_v+T_1)\right) & T_v+T_1\leq t < T_v+T_1+T_2 \\ 0 & T_v+T_1+T_2 < t \end{cases} \tag{12}$$

The jerk limit is used to mitigate any residual vibrations [16], and the jerk signal is obtained by differentiation as

$$j_{i-1}''(t) = \begin{cases} \frac{V_{i-1m}}{T_1T_2} & 0\leq t < T_2 \\ 0 & T_2\leq t < T_1 \\ -\frac{V_{i-1m}}{T_1T_2} & T_1\leq t < T_1+T_2 \\ 0 & T_1+T_2\leq t < T_v \\ -\frac{V_{i-1m}}{T_1T_2} & T_v\leq t < T_v+T_2 \\ 0 & T_v+T_2\leq t < T_v+T_1 \\ \frac{V_{i-1m}}{T_1T_2}t & T_v+T_1\leq t < T_v+T_1+T_2 \\ 0 & T_v+T_1+T_2 < t \end{cases} \tag{13}$$

$$v'''(t) = \begin{cases} \dfrac{V_{i-1m}}{6T_1T_2T_3}\,t^3 & 0 \le t < T_3 \\[2ex] \dfrac{V_{i-1m}}{6T_1T_2}(3t^2 - 3tT_3 + T_3{}^2) & T_3 \le t < T_2 \\[2ex] \dfrac{V_{i-1m}}{6T_1T_2T_3}((3t^2 - 3tT_2 + T_2{}^3 - (t-T_3)^3) & T_2 \le t < T_2 + T_3 \\[2ex] \dfrac{V_{i-1m}}{2T_1}(2t - T_2 - T_3) & T_2 + T_3 \le t < T_1 \\[2ex] \dfrac{V_{i-1m}}{6T_1T_2T_3}(-t^3 - T_1{}^3) + \dfrac{V_{i-1m}}{2T_2T_3}t(T_1 - t) - \dfrac{V_{i-1m}}{2T_1}(2t - T_2 - T_3) & T_1 \le t < T_1 + T_3 \\[2ex] \dfrac{V_{i-1m}}{2T_2}(2t - T_1 - T_3) + \dfrac{V_{i-1m}}{2T_1}(2t - T_2 - T_3) + \dfrac{V_{i-1m}}{6T_1T_2}(3t^2 - 3tT_3 + T_3{}^2) & T_1 + T_3 \le t < T_1 + T_2 \\[2ex] -\dfrac{V_{i-1m}T_1}{6T_2T_3} - \dfrac{V_{i-1m}}{T_3}t - \dfrac{V_{i-1m}T_2}{2T_3} + \dfrac{V_{i-1m}}{2T_2T_3}(t-T_3)^2 & T_1 + T_2 \le t < T_d \\[2ex] \quad -\dfrac{V_{i-1m}}{2T_2T_3}((t - T_2 - T_3)(T_1 - T_2{}^2 - 2T_3 - 2t - (t-T_3)^2) \\[2ex] V_{i-1m} & T_d \le t < T_v \\[2ex] \dfrac{V_{i-1m}}{6T_1T_2T_3}(t^3 - 6T_1T_2T_3 + 3tT_v^2 - 4T_v^3) - \dfrac{V_{i-1m}T_v}{2T_1T_2T_3}(t^2 - T_v^2) & T_v \le t < T_v + T_3 \\[2ex] V_{i-1m}(1 - \dfrac{T_v}{T_1T_2}t + \dfrac{T_vT_3}{2T_1T_2} - \dfrac{3t^2 - 3tT_3 + T_3{}^2}{6T_1T_2} - \dfrac{T_v^2}{2T_1T_2}) & T_v + T_3 \le t < T_v + T_2 \\[2ex] \dfrac{V_{i-1m}}{6T_1T_2T_3}((2T_2^3 - 3T_2^2(T_2 - T_v) + 3T_v(t^2 - 3T_2^2 - 2tT_3 + T_3^2 + 2T_2(t - 2T_v) - T_v^2) & T_v + T_2 \le t < T_v + T_2 + T_3 \\[2ex] \quad + t^3 + 3tT_3^2 - T_3^3 + 3tT_v^2 - 4T_v^3 - 3T_3(t^2 + T_v^2) - 3T_2^2(-t + T_v) + t^2 - 2tT_3 + T_v^2))) \end{cases}$$

$$v'''(t) = \begin{cases} V_{i-1m} - \dfrac{V_{i-1m}}{T_1}(t + T_v) + \dfrac{V_{i-1m}}{2T_1}(T_2 + T_3) & T_v + T_2 + T_3 \le t < T_v + T_1 \\[2ex] \dfrac{V_{i-1m}}{2T_1T_2T_3}((t - T_1 - T_v)(2T_1T_2 + T_2^2 + T_v^2) - (t - T_3 - T_1 - T_v)(2T_1T_2 + T_2^2 + T_2T_v) & T_v + T_1 \le t < T_v + T_1 + T_3 \\[2ex] \quad + (t^2 - (T_1 + T_v)^2(T_2 + T_2T_v + T_1 + T_1T_v - T_v)) + \dfrac{V_{i-1m}}{2T_1T_3}((t - T_3)^2 - (T_1 + T_v)^2) \\[2ex] \quad + \dfrac{V_{i-1m}}{6T_1T_2T_3}(t^3 - (T_1 + T_v)^3) \\[2ex] V_{i-1m} - \dfrac{V_{i-1m}T_v}{2T_1T_2}(2t - T_3 - (T_1 + T_2)(2t - T_3)) - \dfrac{V_{i-1m}}{2T_1T_2}((T_1 + T_2)(2t - T_1 - T_2) & T_v + T_1 + T_3 \le t < T_v + T_1 + T_2 \\[2ex] \quad + \dfrac{V_{i-1m}}{6T_1T_2T_3}(3t^2 - 3T_3\,t + T_3^2)) \\[2ex] \dfrac{V_{i-1m}}{2T_1T_2T_3}((-t + T_d + T_3 + T_v)(T_1T_2 + T_1^2 + T_2^2 + T_v^2) + ((t - T_3)^2) & T_v + T_1 + T_2 \le t < T_v + T_d \\[2ex] \quad - \dfrac{V_{i-1m}}{2T_1T_2T_3}(T_d + T_v)^2)(T_1 + T_2 + T_v + T_1T_v - T_2T_v)) \\[2ex] \quad - \dfrac{V_{i-1m}}{6T_1T_2T_3}((t - T_3)^3 - (T_d + T_v)^3) \\[2ex] 0 & T_v + T_d < t \end{cases}$$

$$
a'''(t) = \begin{cases}
\dfrac{V_m t^2}{2T_1 T_2 T_3} & 0 \le t < T_3 \\[2ex]
\dfrac{V_{i-1m}}{2T_1 T_2}(2t - T_3) & T_3 \le t < T_2 \\[2ex]
-\dfrac{V_{i-1m}}{2T_1 T_2 T_3}(t - T_3)^2 + \dfrac{V_{i-1m}}{T_1 T_3}t - \dfrac{V_{i-1m} T_2}{2T_1 T_3} & T_2 \le t < T_2 + T_3 \\[2ex]
\dfrac{V_{i-1m}}{T_1} & T_2 + T_3 \le t < T_1 \\[2ex]
-\dfrac{V_{i-1m}}{2T_1 T_2 T_3}t^2 + \dfrac{V_{i-1m}}{T_2 T_3}t - \dfrac{V_{i-1m} T_1}{2T_2 T_3} + \dfrac{V_{i-1m}}{T_1} & T_1 \le t < T_1 + T_3 \\[2ex]
-\dfrac{V_{i-1m}}{6T_1 T_2}t + \dfrac{V_{i-1m} T_3}{2T_1 T_2} + \dfrac{V_{i-1m}}{T_1} + \dfrac{V_{i-1m}}{T_2} & T_1 + T_3 \le t < T_1 + T_2 \\[2ex]
\dfrac{V_{i-1m}(t - T_3)^2}{2T_1 T_2 T_3} - \left(\dfrac{1}{T_1 T_3} + \dfrac{1}{T_2 T_3}\right)V_{i-1m}t + V_{i-1m}\left(\dfrac{1}{T_3} + \dfrac{1}{T_1} + \dfrac{1}{T_2} + \dfrac{T_2}{2T_1 T_3} + \dfrac{T_1}{2T_2 T_3}\right) & T_1 + T_2 \le t < T_d \\[2ex]
0 & T_d \le t < T_v \\[2ex]
-\dfrac{V_{i-1m}}{2T_1 T_2 T_3}t^2 - \dfrac{V_{i-1m} T_v}{T_1 T_2 T_3}t - \dfrac{V_{i-1m} T_v^2}{2T_1 T_2 T_3} & T_v \le t < T_v + T_3 \\[2ex]
-\dfrac{V_{i-1m}}{T_1 T_2}t + \dfrac{V_{i-1m} T_3}{2T_1 T_2} - \dfrac{V_{i-1m} T_v}{T_1 T_2} & T_v + T_3 \le t < T_v + T_2 \\[2ex]
V_{i-1m}\left(\dfrac{(t - T_3)^2}{2T_1 T_2 T_3} + \left(\dfrac{T_v}{T_1 T_2 T_3} - \dfrac{1}{T_1 T_3}\right)t + \dfrac{T_2}{2T_1 T_3} + \dfrac{T_v}{T_1 T_3} + \dfrac{T_v^2}{2T_1 T_2 T_3} - \dfrac{T_v}{T_1 T_2}\right) & T_v + T_2 \le t < T_v + T_2 + T_3 \\[2ex]
-\dfrac{V_{i-1m}}{T_1} & T_v + T_2 + T_3 \le t < T_v + T_1
\end{cases}
$$

$$
a'''(t) = \begin{cases}
\begin{aligned}
&V_{i-1m}\left(\dfrac{t^2}{2T_1 T_2 T_3} - \left(\dfrac{1}{T_1 T_3} + \dfrac{1}{T_2 T_3} - \dfrac{1}{T_1 T_3} - \dfrac{T_v}{T_2 T_3} - \dfrac{T_v}{T_1 T_3} + \dfrac{T_v}{T_1 T_2 T_3}\right)t \\
&\quad -\left(\dfrac{T_v}{T_1 T_3} + \dfrac{T_1}{2T_2 T_3} - \dfrac{1}{T_1} + \dfrac{T_v^2}{2T_1 T_2 T_3}\right)\Big)
\end{aligned} & T_v + T_1 \le t < T_v + T_1 + T_3 \\[2ex]
V_{i-1m}\left(\dfrac{t}{T_1 T_2} - \dfrac{1}{T_1} - \dfrac{1}{T_2} + \dfrac{T_v}{T_1} + \dfrac{T_v}{T_2} - \dfrac{T_3}{2T_1 T_2} - \dfrac{T_v}{T_1 T_2}\right) & T_v + T_1 + T_3 \le t < T_v + T_1 + T_2 \\[2ex]
\begin{aligned}
&-\dfrac{V_{i-1m}(t - T_3)^2}{2T_1 T_2 T_3} + \left(\dfrac{1}{T_1 T_3} - \dfrac{T_v}{T_1 T_3} + \dfrac{1}{T_2 T_3} - \dfrac{T_v}{T_2 T_3} + \dfrac{T_v}{T_1 T_2 T_3}\right)V_{i-1m}t \\
&\quad +\left(-\dfrac{1}{T_3} + \dfrac{1}{T_2} + \dfrac{1}{T_1} + \dfrac{T_v}{T_2} + \dfrac{T_v}{T_1} - \dfrac{T_v}{T_1 T_2} - \dfrac{T_1}{2T_2 T_3} - \dfrac{T_v^2}{2T_1 T_2 T_3} - \dfrac{T_2}{2T_1 T_3}\right)V_{i-1m}
\end{aligned} & T_v + T_1 + T_2 \le t < T_v + T_d \\[2ex]
0 & T_v + T_d < t
\end{cases}
$$

The trapezoid velocity signal is convoluted once to generate a smooth curve, and the velocity is differentiated to obtain acceleration and jerk. The whole processing time is $T_{all} = T_v + T_1 + T_2$, and delay time is $T_d = T_1 + T_2$.

Under the condition of only considering $T_v > T_1 + T_2 + T_3$ and $T_1 > T_2 + T_3$, the velocity expression of triple filtering is written as

The acceleration profile in Fig. 5 can be written as

$$
j'''(t) = \begin{cases}
\dfrac{V_m \, t}{T_1 T_2 T_3} & 0 \le t < T_3 \\[2mm]
\dfrac{V_{i-1m}}{T_1 T_2} & T_3 \le t < T_2 \\[2mm]
-\dfrac{V_{i-1m}}{T_1 T_2 T_3}(t - T_3) + \dfrac{V_{i-1m}}{T_1 T_3} & T_2 \le t < T_2 + T_3 \\[2mm]
0 & T_2 + T_3 \le t < T_1 \\[2mm]
-\dfrac{V_{i-1m}}{T_1 T_2 T_3} t + \dfrac{V_{i-1m}}{T_2 T_3} & T_1 \le t < T_1 + T_3 \\[2mm]
-\dfrac{V_{i-1m}}{6 T_1 T_2} & T_1 + T_3 \le t < T_1 + T_2 \\[2mm]
\dfrac{V_{i-1m}(t - T_3)}{T_1 T_2 T_3} - \left(\dfrac{1}{T_1 T_3} + \dfrac{1}{T_2 T_3}\right)V_{i-1m} & T_1 + T_2 \le t < T_d \\[2mm]
0 & T_d \le t < T_v \\[2mm]
-\dfrac{V_{i-1m}}{T_1 T_2 T_3} t - \dfrac{V_{i-1m} T_v}{T_1 T_2 T_3} & T_v \le t < T_v + T_3 \\[2mm]
-\dfrac{V_{i-1m}}{T_1 T_2} & T_v + T_3 \le t < T_v + T_2 \\[2mm]
V_{i-1m}\left(\dfrac{t - T_3}{T_1 T_2 T_3} + \left(\dfrac{T_v}{T_1 T_2 T_3} - \dfrac{1}{T_1 T_3}\right)\right) & T_v + T_2 \le t < T_v + T_2 + T_3 \\[2mm]
0 & T_v + T_2 + T_3 \le t < T_v + T_1 \\[2mm]
V_{i-1m}\left(\dfrac{t}{T_1 T_2 T_3} - \left(\dfrac{1}{T_1 T_3} + \dfrac{1}{T_2 T_3} - \dfrac{1}{T_1 T_3} - \dfrac{T_v}{T_2 T_3} - \dfrac{T_v}{T_1 T_3} + \dfrac{T_v}{T_1 T_2 T_3}\right)\right) & T_v + T_1 \le t < T_v + T_1 + T_3 \\[2mm]
\dfrac{V_{i-1m} t}{T_1 T_2} & T_v + T_1 + T_3 \le t < T_v + T_1 + T_2 \\[2mm]
-\dfrac{V_{i-1m}(t - T_3)}{T_1 T_2 T_3} + \left(\dfrac{1}{T_1 T_3} - \dfrac{T_v}{T_1 T_3} + \dfrac{1}{T_2 T_3} - \dfrac{T_v}{T_2 T_3} + \dfrac{T_v}{T_1 T_2 T_3}\right)V_{i-1m} & T_v + T_1 + T_2 \le t < T_v + T_d \\[2mm]
0 & T_v + T_d < t
\end{cases}
$$

where the jerk signal is obtained by differentiation as:

The original rectangular pulse is convoluted three times to produce a smooth curve in Fig. 5. The whole processing time is $T_{all} = T_v + T_1 + T_2 + T_3$, and delay time is $T_d = T_1 + T_2 + T_3$. The curves of velocity, acceleration, and jerk are smoother than the original curves.

2.2 Accurate interpolation and contouring control algorithm for the corner transition

In high-speed machining, the continuous feed pulse can produce uninterrupted motion, and the interpolation with FIR filter will inevitably produce delay. In this paper, an algorithm is proposed, which need not to wait until the filter delay time is completed. The research adjusts the delay time to precisely control the contour error of the corner.

First, overlap time is defined as

$$0 \le T_n \le T_d \tag{17}$$

If $T_n = 0$, a P2P trajectory is generated as shown in Fig. 6a. If $T_n = T_d/2$, consecutive interpolation is initiated before feed motion of the first short segment comes to a full stop. Contour errors are shown in Fig. 6b at the corner.

The research methods of X-axis and Y-axis are similar, and X-axis is taken as an example. If $T_n > 0$, X-axis velocity changes profile in Fig. 7. The processing time of the first section $P_{i-1}P_i$ is $t = T_v + T_d$, but the start time of the second paragraph $P_i P_{i+1}$ is $t = T_v + T_d - T_n$ in Fig. 7. The bisector of the maximum deviation node occurs at $t = T_v + T_d - T_n/2$. The research method is used to determine the corner contour error. V_{sx} is velocity of X-axis entering the corner transfer point; V_{sy} is velocity of Y-axis entering the corner transfer point. V_{ex} is velocity of X-axis leaving corner transfer point; V_{ey} is velocity
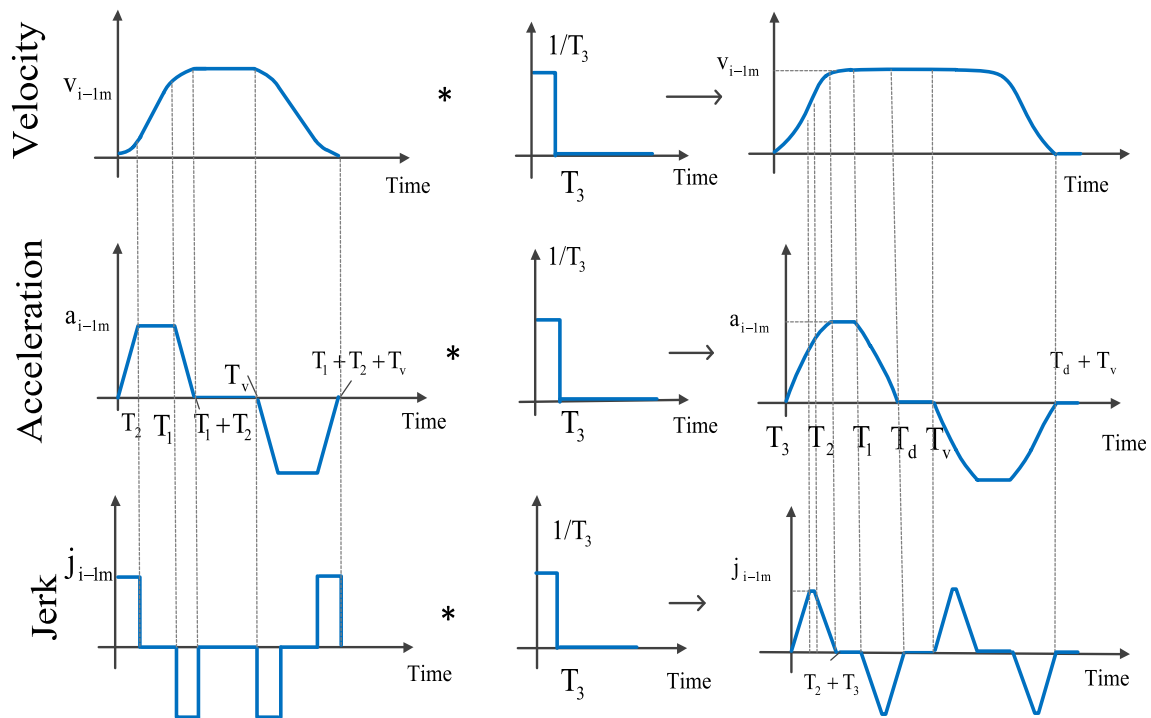
Fig. 5 Each parameter profile by the third-order FIR filter

of Y-axis leaving corner transfer point. α_0 is the angle between $P_{i-1}P_i$ and X-axis, γ_0 is the angle between P_iP_{i+1} and X-axis, φ_0 is the angle between $P_{i-1}P_i$ and P_iP_{i+1}, and ε is contour error.

Relation the velocity of transition point and the maximum feed velocity is written as

$$\begin{aligned} V_{sx} &= V_{i-1m}\cos(\alpha) & V_{sy} &= V_{i-1m}\sin(\alpha) \\ V_{ex} &= V_{im}\cos(\gamma) & V_{ey} &= V_{im}\sin(\gamma) \end{aligned} \quad (18)$$

In order to facilitate the study, assuming $V_{i-1m} = V_{im} = V_m$, according to Eq. (15), the maximum contour error can be written as
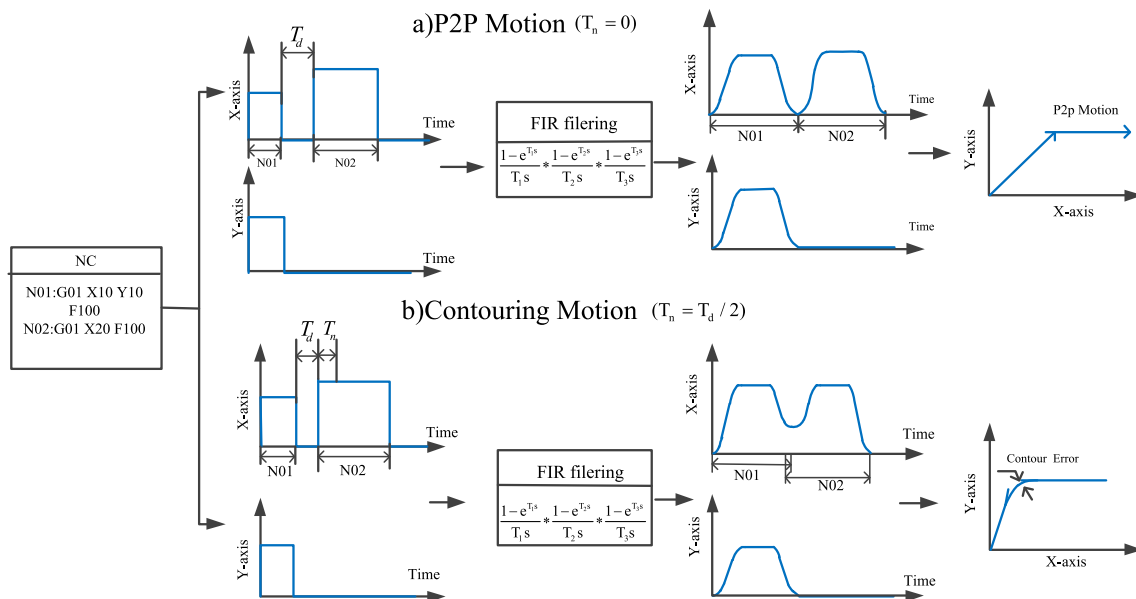
Fig. 6 Continuous short line interpolation strategy for the corner

Fig. 7 Contour error diagram of corner contour
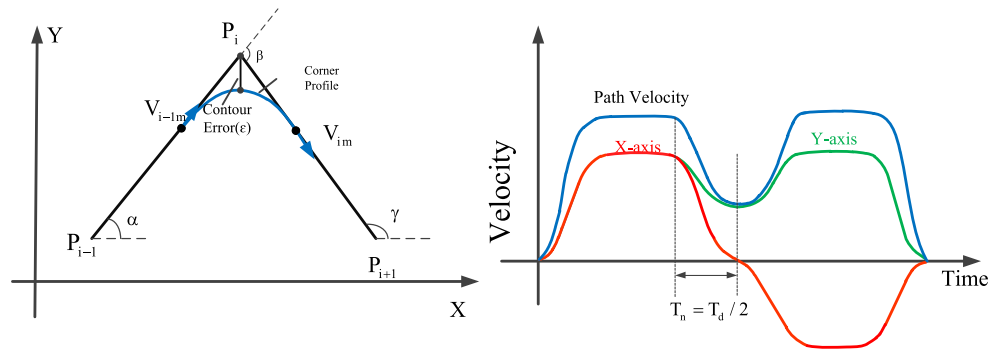
$$\varepsilon = \begin{cases} \dfrac{V_m T_n^4}{192 T_1 T_2 T_3} \sin(\beta/2) & 0 \le T_k \le 2T_3 \\ \dfrac{V_m\left(-2T_3^3 + 4T_3^2 T_n - 3T_3 T_n^2 + T_n^3\right)}{24 T_1 T_2} \sin(\beta/2) & 2T_3 < T_k \le T_1 + T_3 \end{cases}$$

(19)

Finally, the overlapping time can be solved from Eq. (19) as

$$k = -\frac{108 \varepsilon \sin(\beta/2) T_1 T_2}{V_m} + \frac{\sqrt{11664 \varepsilon \sin^2(\beta/2) T_1^2 T_2^2 + 3 V_m^2 T_3^6}}{V_m}$$

$$T_n = \begin{cases} \sqrt[4]{\dfrac{192 T_1 T_2 T_3 \, \varepsilon}{V_m \sin(\beta/2)}} & 0 \le T_k \le 2T_3 \\ T_3 + \dfrac{T_3^2}{3^{1/3}(k)^{1/3}} - \dfrac{k^{1/3}}{3^{2/3}} & 2T_3 < T_k \le T_1 + T_3 \end{cases}$$

(20)

With this algorithm, the contour error of the corner can be accurately controlled. The flow chart is shown in Fig. 8.
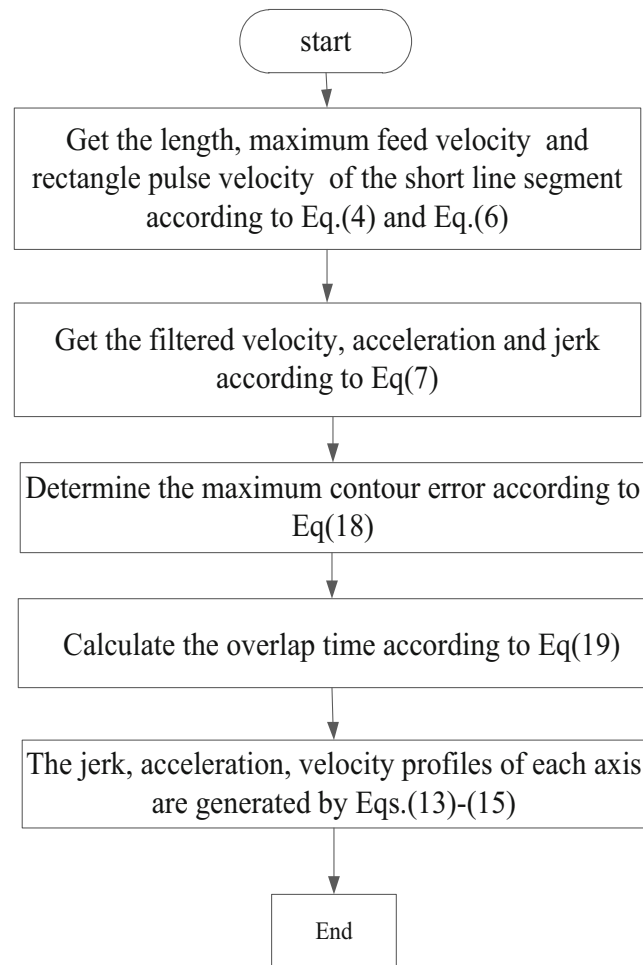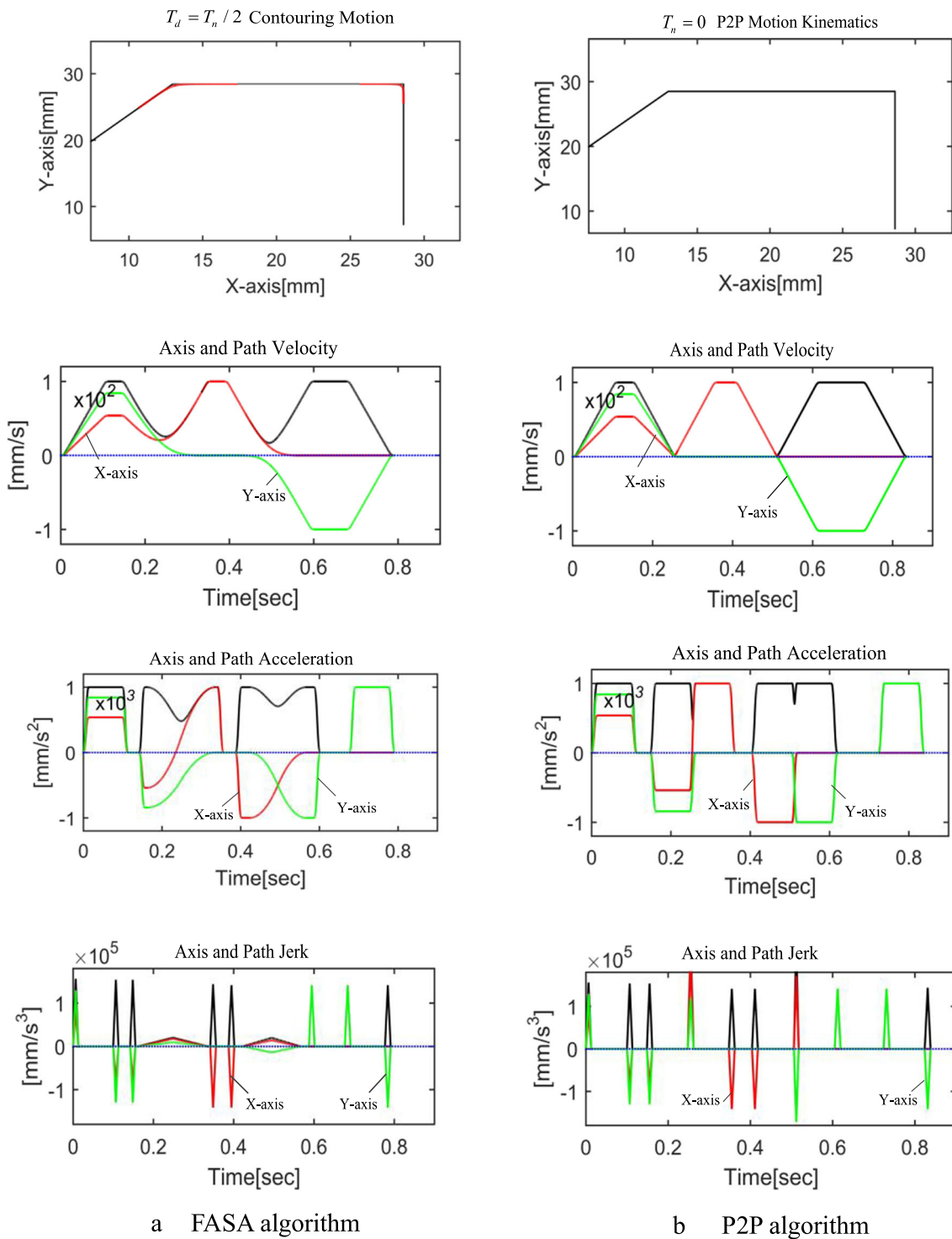

Fig. 8 Accurate interpolation and contouring control algorithm

a FASA algorithm   b P2P algorithm

Fig. 9 **a** FASA algorithm. **b** P2P algorithm

3 Simulation and experimental results

In this paper, an accurate interpolation and contouring control algorithm based on FIR filters for the corner transition is proposed. This algorithm can accurately control the contour error of the corner. Next, the point-to-point algorithm and the algorithm proposed in this paper are analyzed in detail to verify the superiority of the algorithm.
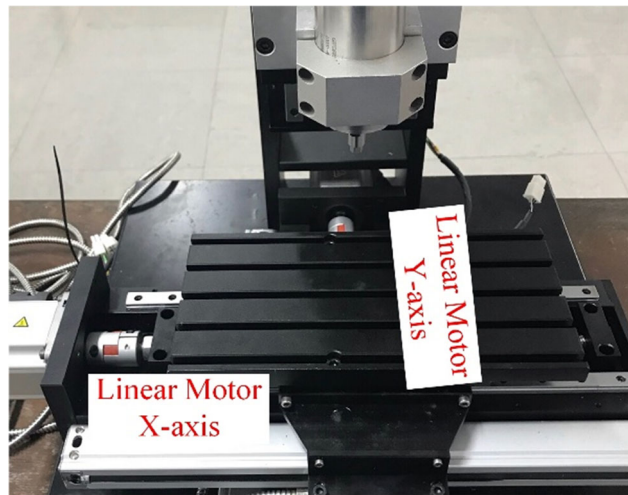
Fig. 10 Experimental setup

3.1 Simulation results

As shown in Fig. 9, tool paths are the obtuse angle of 123 and the right angle; an analysis with zero overlap time and half of the delay time is performed. The total length of the path is 51.64 mm. The feed along the tool path is set to $V_m = 100$ mm/s, and 3 FIR filters are used with time constants $T_1 = 20$ ms, $T_2 = 10$ ms, and $T_3 = 5$ ms. The maximum interpolation error tolerance is 10 μm. The precise algorithm of high-speed machining corner based on FIR filter is abbreviated to FASA. The path is interpolated based on FASA in Fig. 9a.

The delay time during simulation is 35 ms, the contour error around segment transitions is controlled by calculating the overlapping time T_n based on the change in the feed direction from Eq. (20). The total processing time is

0.7907 s. After the speed at the corner need not to be reduced to zero, the transfer is carried out. There is no additional deceleration time. The velocity at the obtuse angle is 28.96 mm/s, the speed at the acute angle is 21.67 mm/s. The jerk can be processed within the limit range, and the generated acceleration can reach G^1 continuous. The path is interpolated based on P2P in Fig. 9b. Total machining time is 0.8296; speed needs to be reduced to zero before transferring. The phenomenon of exceeding the jumping limit occurs in the process of machining, and this will cause tool vibration and reduce the surface quality of machined parts.

By comparing FASA and P2P algorithm, the proposed algorithm can accurately determine contour error of corner, make acceleration at the corner reach G^1 continuous, and reduce vibration of tool at corner.
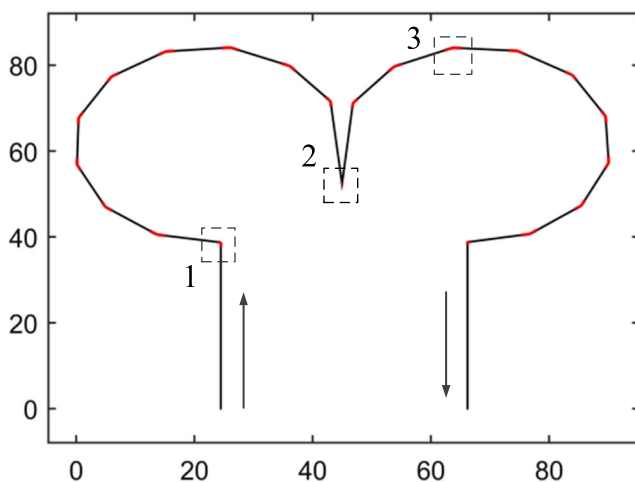
3.2 Experimental results

The kinematic performance of the corner contour algorithm is analyzed by experiments; the equipment is an X-Y CNC machine tool driven by two motors shown in Fig. 10. The resolution of linear encoder is 0.8 μm. The feedback bandwidth of axis position is 50 Hz, which can ensure good position synchronization and path tracking. The feed velocity is set to $V_m = 100$ mm/s, and 3 FIR filters are used with time constants $T_1 = 20$ ms, $T_2 = 10$ ms, and $T_3 = 5$ ms. The maximum contour error is 20 μm; acceleration and jerk of motor driver are limited to $J_m = 1.5 \times 10^5$ mm/s^4, $A_m = 1000$ mm/s^2, respectively. This algorithm is compared with NURBS and P2P algorithms. Tool path is shown in Fig. 11; corner enlarged is shown in Fig. 12. The enlarged angles on the three corner profiles are 103, 32 and 156.
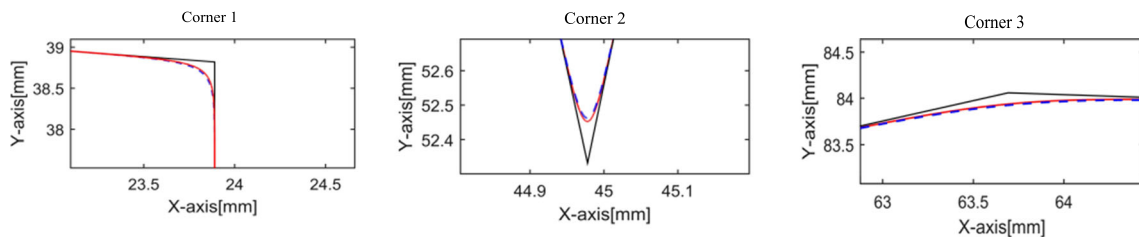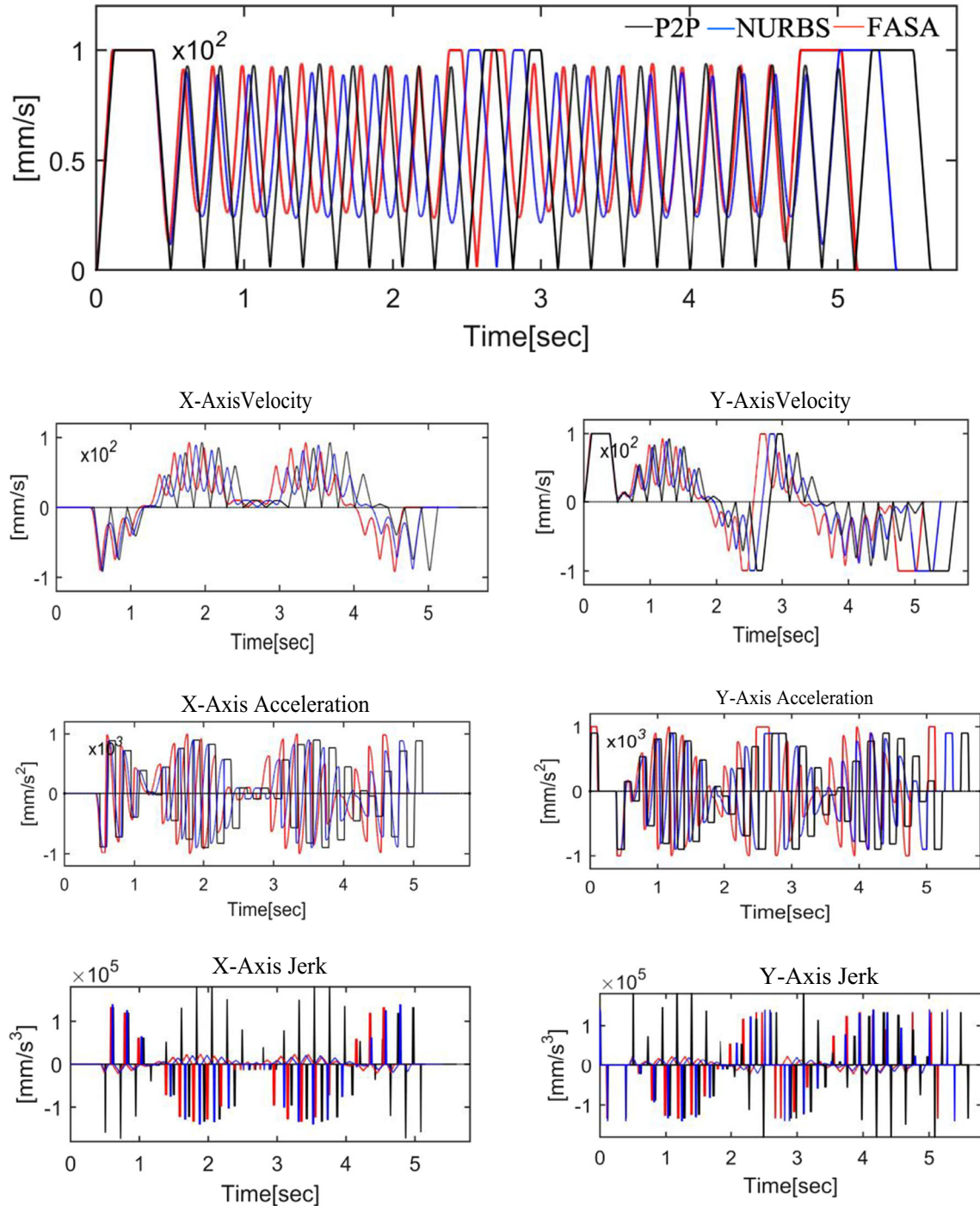

Fig. 11 Tool path

Fig. 12 Corner zoom

**Fig. 13** Velocity, acceleration, and jerk profiles in experiment

Table 1 Comparison of various algorithms

Algorithms	Machining time [s]	Velocity profile	Acceleration profile	Contour error MAX [um]
FASA	5.1021	G^2 continuity	G^1 continuity	21.09
NURBS	5.4989	G^2 continuity	G^1 continuity	23.68
P2P	5.6701	G^1 continuity	Discontinuity	0

The experimental velocity, acceleration, and jerk profile is shown in Fig. 13. Machining time and contouring performance comparison are shown in Table 1. As noted from Table 1, the machining time of NURBS algorithm is 5.4989 s, the machining time of P2P algorithm is 5.6701 s, and the machining time of FASA algorithm is 5.1021 s; FASA algorithm takes the shortest time, which can effectively improve the processing efficiency. FASA algorithm has the minimum change range of jerk profiles. The P2P algorithm exceeds the jerk limit in the process of machining, which causes the vibration of cutting tool and affects the quality of machining surface. The maximum contour error of FASA algorithm is 21.09 μm, and FASA algorithm is smaller than the maximum contour error of NURBS algorithm (Fig. 14).

4 Conclusions

The sharp corner of the short line segment will have sudden change in speed, which will cause the violent vibration of the machining tool and affect the surface quality of the machined parts. The pulse response technology can realize the smooth transition of the corner, but the pulse response technology can not accurately control the maximum contour error. In this paper, an accurate interpolation and contouring control algorithm for the corner transition is proposed by using FIR filter, which can effectively control the corner contour error and realize smooth transition. The maximum contour of the corner
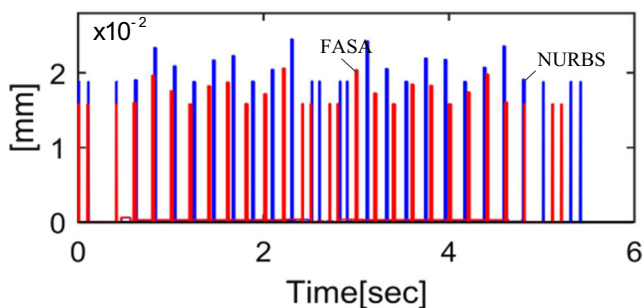
is determined by overlapping time, and different overlapping time produces different tool trajectories. Through simulation and experimental analysis, FASA algorithm can start transmitting around the corner without reducing velocity to zero. The total processing time is relatively short, the vibration and impact generated by the tool at the corner is small, and the processing quality is improved. Compared with point-to-point (P2P) and NURBS algorithm, the algorithm proposed in this paper can reduce the machining time by 7–10% and effectively reduce the maximum contour error of the vibration corner of the tool.

References

1. Moetakef Imani B, Ghandehariun A (2011) Real-time PH-based interpolation algorithm for high speed CNC machining. Int J Adv Manuf Technol 56(5):619–629
2. Sun S, Lin H, Zheng L (2016) A real-time and look-ahead interpolation methodology with dynamic B-spline transition scheme for CNC machining of short line segments. Int J Adv Manuf Technol 84(5):1359–1370
3. Zhang J, Zhang L, Zhang K (2015) Double NURBS trajectory generation and synchronous interpolation for five-axis machining based on dual quaternion algorithm. Int J Adv Manuf Technol 83(9–12):2015–2025
4. Ernesto CA, Farouki RT (2012) High-speed cornering by CNC machines under prescribed bounds on axis accelerations and toolpath contour error. Int J Adv Manuf Technol 58:327–338
5. Duan M, Okwudire C (2016) Minimum-time cornering for CNC machines using an optimal control method with NURBS parameterization. Int J Adv Manuf Technol 85(5):1405–1418
6. Biagiotti L, Melchiorri C (2012) FIR filters for online trajectory planning with time- and frequency-domain specifications. Control Eng Pract 20(12):1385–1399
7. Chen CS, Lee AC (1998) Design of acceleration/deceleration profiles in motion control based on digital FIR filters. Int J Mach Tool Manu 38(7):799–825
8. Kim DI, Jeon J, Kim S (1994) Software acceleration/deceleration methods for industrial robots and CNC machine tools. MECHATRONICS 4:37–53
9. Jeon JW, Ha YY (2000) A generalized approach for the acceleration and deceleration of industrial robots and CNC machine tools. IEEE Trans Ind Electron 47:133–139

Fig. 14 Measured contour errors in experiment

10. Sencer B, Ishizaki K, Shamoto E (2015) High speed cornering strategy with confined contour error and vibration suppression for CNC machine tools. CIRP Ann Manuf Technol 64(1):369–372

11. Besset P, Béarée R (2017) FIR filter-based online jerk-constrained trajectory generation. Control Eng Pract 66:169–180

12. Béarée R, Olabi A (2013) Dissociated jerk-limited trajectory applied to time-varying vibration reduction. Robot Comput Integr Manuf 29(2):444–453

13. Altintas Y, Khoshdarregi MR (2012) Contour error control of CNC machine tools with vibration avoidance. CIRP Ann Manuf Technol 61(1):335–338

14. Erkorkmaz K, Altintas Y (2001) High speed CNC system design. Part I: jerk limited trajectory generation and quintic spline interpolation. Int J Mach Tool Manu 41(9):1323–1345

15. Tajima S, Sencer B, Shamoto E (2018) Accurate interpolation of machining tool-paths based on FIR filtering. Precis Eng 52:332–344

16. Pierre-Jean B, Richard B, Pierre B (2005) Influence of a jerk controlled movement law on the vibratory behaviour of high-dynamics systems. J Intell Robot Syst 42(3):275–293

Publisher's note Springer Nature remains neutral with regard to jurisdictional claims in published maps and institutional affiliations.